Ab Initio Optical Potentials and Nucleon Scattering on Medium Mass Nuclei

A. Idini,[1,2] C. Barbieri,[1] and P. Navrátil[3]

[1]*Department of Physics, University of Surrey, Guildford GU2 7XH, United Kingdom*
[2]*Division of Mathematical Physics, Department of Physics, LTH, Lund University, P.O. Box 118, S-22100 Lund, Sweden*
[3]*TRIUMF, 4004 Wesbrook Mall, Vancouver, British Columbia V6T 2A3, Canada*

We derive *ab initio* optical potentials from self-consistent Green's function theory and compute the elastic scattering of neutrons off oxygen and calcium isotopes. The comparison with scattering data is satisfactory at low scattering energies. The method is benchmarked against the no-core shell model with continuum calculations, showing that virtual excitations of the target are crucial to predict proper fragmentation and absorption at higher energies. This is a significant step toward deriving optical potentials for medium mass nuclei and complex many-body systems in general.

Introduction.—Reactions are a fundamental aspect of nuclear physics since they are used experimentally to determine many properties of atomic nuclei. They are also a key component to significant scientific questions, such as the reaction networks that control nucleosynthesis. Unfortunately, first principles theoretical descriptions for scattering on medium mass nuclei are still lacking. Even though ground state properties and excited states can be calculated *ab initio*, the complexity of many-body dynamics forces us to model the reaction mechanisms in terms of phenomenological optical potentials. This lack of consistency among the structure and reaction theories has been a major issue for nuclear physics for decades.

Optical models are an effective way to decouple the scattering wave function of the projectile from the internal structure of the target. Thus, microscopic (nonphenomenological) formalisms have also been proposed to compute them [1,2], although working implementations are still scarce. In this Letter, we discuss an *ab initio* calculation of optical potentials that starts from saturating nuclear forces and compares favorably with low-energy scattering data. In doing so, we also identify key ingredients needed to improve the predictability at higher energies. This represents a successful step toward gaining insight into the reaction dynamics and to performing reliable predictions of scattering with exotic nuclei.

Many-body Green's function methods are particularly suited to pursue this goal for medium and heavy nuclei since their central quantity, the self-energy, is naturally linked to the Feshbach theory of optical potentials [1,3]. While the particle part of the self-energy is equivalent to the original formulation of Feshbach, its hole part also describes the structure of the target [2]. Hence, it facilitates a consistent treatment of scattering and structure.

Some related (semi)phenomenological attempts to exploit Green's function methods include the nuclear field theory [4,5] and its extension to nuclear transfer reactions [6,7]. Another incarnation of Green's function related theories is the dispersive optical model [8], which is a data driven formulation of global (local and nonlocal) potentials constructed as the best possible parametrization of a microscopic self-energy [9,10]. The nuclear structure method was applied recently obtaining good reproduction of ^{40}Ca scattering based on the Gogny D1S interaction [11]. Other approaches based on the nucleon-nucleon T-matrix and folding with the nuclear density have proven to be effective [12–15].

Ab initio methods have been successful in direct calculations of scattering when only a few nucleons are at play. Quantum Monte Carlo calculations have been historically used for light nuclei [16–18]. The no-core shell model with resonating group method (NCSM-RGM) or with continuum (NCSMC) have been successful in calculating scattering and transfer reactions for light targets [19–21]. Coupled cluster theory has also been employed with a Gamow basis for proton scattering from ^{40}Ca [22] and combined with a Green's function approach to compute phase shifts for ^{16}O and Ca isotopes [23,24]. On the other hand, the self-consistent Green's function (SCGF) formalism [25,26] can calculate the microscopic optical potential directly even for heavier nuclei. This approach has been used to compute phase shifts [27] and to investigate analytical properties of optical models [28]. However, these early studies were limited to two-nucleon (NN) forces, and a comparison to the experiment has been hindered by the lack of realistic Hamiltonians capable of reproducing the radius of the target.

Three-nucleon (3N) interactions were recently formulated and implemented for SCGF theory in Refs. [29–31]. Moreover, the introduction of saturating nuclear interactions [32] has allowed for a good reproduction of radii and binding energies across the oxygen [33] and calcium

chains [34]. Hence, we are now in a position to meaningfully compare first principles approaches to scattering data in medium mass nuclei. In the following, we present state-of-the-art SCGF calculations to test current *ab initio* methods and compare our results to NCSM-RGM and NCSMC computations with NN and NN $+ 3N$ interactions. We then use a saturating chiral Hamiltonian to study elastic scattering of neutrons from ^{16}O and ^{40}Ca.

Formalism.—The Hamiltonian used to compute the self-energy is

$$H(A) = \hat{T} - \hat{T}_{\text{c.m.}}(A + 1) + \hat{V} + \hat{W}, \quad (1)$$

where $\hat{T}_{\text{c.m.}}(A + 1)$ is the center of mass kinetic energy for the A-nucleon target plus the projectile, and $\hat{V}$ and $\hat{W}$ are the NN and 3N interactions. $\hat{W}$ is included as an equivalent effective two-body interaction, averaged on the correlated propagator as discussed in Refs. [30,35]. The SCGF calculation proceeds by solving the Dyson equation, $g(\omega) = g^0(\omega) + g^0(\omega)\Sigma^\star(\omega)g(\omega)$, in a harmonic oscillator (HO) basis of $N_{\text{max}} + 1$ shells, where $g^0(\omega)$ is the free particle propagator, and the irreducible self-energy $\Sigma^\star(\omega)$ has the following general spectral representation:

$$\Sigma^\star_{\alpha\beta}(E,\Gamma) = \Sigma^{(\infty)}_{\alpha\beta} + \sum_{i,j} \mathbf{M}^\dagger_{\alpha,i}\left(\frac{1}{E - (\mathbf{K}^> + \mathbf{C}) + i\Gamma}\right)_{i,j} \mathbf{M}_{j,\beta}$$
$$+ \sum_{r,s} \mathbf{N}_{\alpha,r}\left(\frac{1}{E - (\mathbf{K}^< + \mathbf{D}) - i\Gamma}\right)_{r,s} \mathbf{N}^\dagger_{s,\beta}, \quad (2)$$

where α and β label the single particle quantum numbers of the HO basis, $\Sigma^{(\infty)}$ is the correlated and energy independent mean field, and Γ sets the correct boundary conditions. We performed calculations with the third order algebraic diagrammatic construction [ADC(3)] method, where the matrix $\mathbf{M}$ ($\mathbf{N}$) couples single particle states to intermediate $2p1h$ ($2h1p$) configurations, $\mathbf{C}$ ($\mathbf{D}$) is the interaction matrix among these configurations, and $\mathbf{K}$ contains their unperturbed energies [36,37]. All intermediate $2p1h$ and $2h1p$ states (respectively labeled by indices i, j and r, s) were included. For $N_{\text{max}} = 13$, this incorporates configurations up to 400 MeV of excitation energy and partial waves of the projectile up to angular momentum $j = 27/2$ for both parities.

The resulting dressed single particle propagator can be written in the Källén-Lehmann representation as

$$g_{\alpha\beta}(E,\Gamma) = \sum_n \frac{\langle\Psi^A_0|c_\alpha|\Psi^{A+1}_n\rangle\langle\Psi^{A+1}_n|c^\dagger_\beta|\Psi^A_0\rangle}{E - E^{A+1}_n + E^A_0 + i\Gamma}$$
$$+ \sum_k \frac{\langle\psi^A_0|c^\dagger_\alpha|\Psi^{A-1}_k\rangle\langle\Psi^{A-1}_k|c_\beta|\Psi^A_0\rangle}{E - E^A_0 + E^{A-1}_k - i\Gamma}. \quad (3)$$

The poles of the forward-in-time propagator, $E^{A+1}_n - E^A_0$, indicate then the energy of the nth exited state of the

$(A + 1)$-nucleon system with respect to the ground state of the target A. Hence, they are directly identified with the scattering energy. For each many-body state $|\Psi^{A+1}_n\rangle$ in the continuum, the corresponding overlaps $\psi_n(\alpha) \equiv \langle\Psi^{A+1}_n|c^\dagger_\alpha|\Psi^A_0\rangle$ are associated with the elastic scattering wave function through Feshbach theory [1,38].

Although the scattering waves are unbound, the self-energy $\Sigma^\star(\omega)$ associated with the optical potential is localized, and it can be efficiently expanded on square integrable functions. Hence, we proceed by calculating Eq. (2) in HO basis but transform it to momentum space before solving the scattering problem. This will ensure that the proper asymptotic behaviors of both bound and scattering states are obtained. The optical potential for a given partial wave (l, j) is then expressed as

$$\Sigma^{\star l,j}(k, k'; E, \Gamma) = \sum_{n,n'} R_{n,l}(k)\Sigma^{\star l,j}_{n,n'}(E, \Gamma)R_{n',l}(k'), \quad (4)$$

which is nonlocal and energy dependent, where $R_{n,l}(k)$ are the radial HO wave functions in momentum space. Through Eqs. (2) and (4), the SCGF approach provides a parametrized, separable, and analytical form of the optical potential.

The parameter Γ sets the time ordering boundary conditions, but it does not affect the solution of the many-body problem that comes from the diagonalization of the equation of motion [5,27,37]. However, we retain it in Eq. (4) to introduce a small finite width for the $2p1h$ and $2h1p$ configurations, which would otherwise be discretized in the present approach. We checked that this does not affect our conclusions below.

We use the intrinsic Hamiltonian of Eq. (1) and large enough HO spaces so that the intrinsic ground state decouples from the center of mass motion [39]. Even if decoupled, the latter is not fully suppressed and the self-energy (4) is still computed in laboratory frame. We correct for this by rescaling the scattering momentum appropriately, which naturally leads to the correct center of mass (c.m.) energy $E_{\text{c.m.}}$ and reduced mass $\mu = \gamma m$, with $\gamma \equiv A/(A+1)$. The Dyson equation eventually reduces to the following one-body eigenvalue problem [25,37]:

$$[E_{\text{c.m.}} - k^2/(2\mu)]\psi_{l,j}(k)$$
$$= \int dk' k'^2 \gamma^3 \Sigma^{\star l,j}(\gamma k, \gamma k'; \gamma E_{\text{c.m.}}, \Gamma)\psi_{l,j}(k'), \quad (5)$$

We diagonalize this Schrödinger-like equation in momentum space so that the kinetic energy is treated exactly and we account for the nonlocality and l, j dependence of Eq. (4). The phase shifts $\delta(E_{\text{c.m.}})$ are obtained as a function of the projectile energy for each partial wave, from which the differential cross section can be calculated. The bound state solutions of Eq. (5) yields overlap wave functions between $|\Psi^A\rangle$ and $|\Psi^{A+1}\rangle$ [40]. Hence, they provide
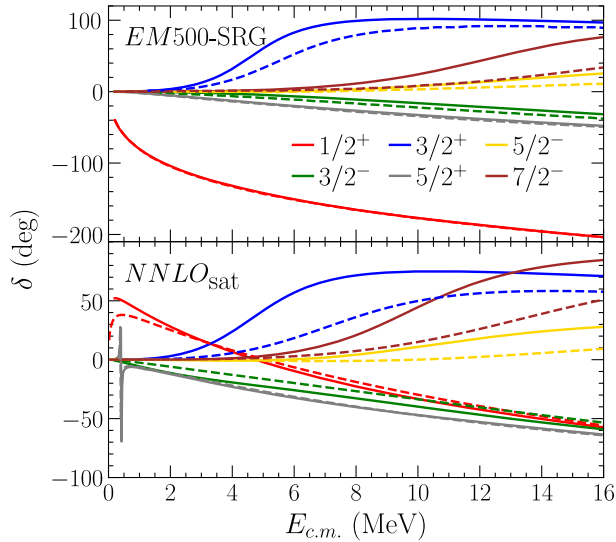
FIG. 1. Real part of nuclear phase shifts, $\delta(E_{\text{c.m.}})$, for neutrons scattering off ^{16}O as a function of energy obtained from the (upper panel) EM500-SRG and (lower panel) NNLO$_{\text{sat}}$ interactions. The solid lines are SCGF calculations using only the static part of the self-energy $\Sigma^{(\infty)}$ in a $N_{\text{max}} = 13$ space. The dashed lines are for NCSM-RGM, which included only the ground state of ^{16}O and used a no-core model space up to (top, from Ref. [19]) $N_{\text{NCSM}} = 18\hbar\Omega$ and (bottom) $8\hbar\Omega$.

spectroscopic factors and asymptotic normalization coefficients that can be employed for the consistent computation of nucleon capture and knockout processes.

Results.—We first compare to early NCSM-RGM results from Ref. [19], where neutron scattering off ^{16}O was computed with a NN-only interaction derived from the chiral next-to-next-to-next-to-leading order force of Ref. [41] (EM500) and evolved with free space similarity renormalization group (SRG) [42] to a cutoff $\lambda = 2.66$ fm^{-1}. This soft interaction facilitates model space convergence and allows for a more meaningful benchmark. These early NCSM-RGM computations did not include virtual excitations of the target nucleus. For consistence, we performed our SCGF calculations with the same Hamiltonian but evaluated the phase shifts using only the static self-energy, $\Sigma^{(\infty)}$. The comparison is shown in the upper panel of Fig. 1, and it is very satisfactory for the $j^\pi = 1/2^+$ and $5/2^+$ partial waves. For this light nucleus, the discrepancy of about 1 MeV for the energy of the $3/2^+$ resonance is also consistent with the uncertainty in the transformation to the center of mass system done in Eq. (5). As we discuss below, doorway excitations of the target nucleus have a strong impact on the energies of single particle resonances. To account for this, we performed new NCSMC calculations that can also include low-lying excitations of ^{17}O. Extrapolating from model spaces of $N_{\text{NCSM}} = 6$–$10\hbar\Omega$, we find quasiparticle energies of -3.4, -2.7, and 3.2 MeV for the $5/2^+, 1/2^+$ bound states and the $3/2^+$ resonance, respectively. The corresponding results from the SCGF, including the full $\Sigma^\star(\omega)$ self-energy, are
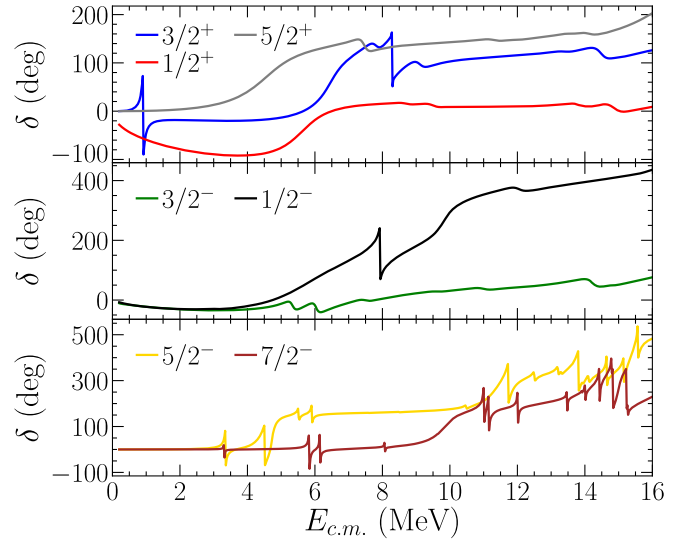
FIG. 2. Real phase shifts, $\delta(E_{\text{c.m.}})$, for neutrons scattering off ^{16}O using the complete self-energy, Eq. (2), and NNLO$_{\text{sat}}$ in an oscillator space of frequency $\hbar\Omega = 20$ MeV and size $N_{\text{max}} = 13$. (Upper panel) Positive parity, (central panel) $l = 1$, and (lower panel) $l = 3$ partial waves are shown.

-6.3, -5.5, and 0.5 MeV. These should be expected to be more bound since SCGF introduces a larger number of $2p1h$ doorway configurations. At the same, time the excitation energies relative to the ^{17}O ground state agree to within 200 keV, which is a satisfactory agreement given the different many-body truncations of the two approaches.

We performed an analogous comparison for the chiral next-to-next-to-leading order $NN + 3N$ interaction of Ref. [32] (named NNLO$_{\text{sat}}$). For NCSM techniques, ^{16}O is more difficult to converge because the interaction is harder and the additional $3N$ matrix elements limit the applicability of importance truncation [43]. We performed our NCSM-RGM calculations at $N_{\text{NCSM}} = 8\hbar\Omega$ and estimated an uncertainty of 1 to 2 MeV for the position of resonances. The SCGF still allows computations with $N_{\text{max}} = 13$, and we find that phase shifts are well converged up to 15 MeV for this space. This puts into evidence the advantage of the latter approach to address *ab initio* scattering off medium mass isotopes. The NNLO$_{\text{sat}}$ benchmark is displayed in the lower panel of Fig. 1, and it is qualitatively similar to the case of the soft EM500-SRG interaction, with the $j^\pi = 1/2^+$ and $5/2^+$ waves agreeing best. For both Hamiltonians, the largest discrepancies are for the $j^\pi = 3/2^+$ and $7/2^-$ resonances, which are more affected by correlations in the continuum and the different many-body truncations of the two approaches. NNLO$_{\text{sat}}$ was explicitly constructed to reproduce correct nuclear saturation properties of medium mass nuclei, including binding energies and radii. The constraint on radii is crucial to predicting elastic scattering observables that can be reasonably compared to the experiment; hence, we will focus on this Hamiltonian in the following.
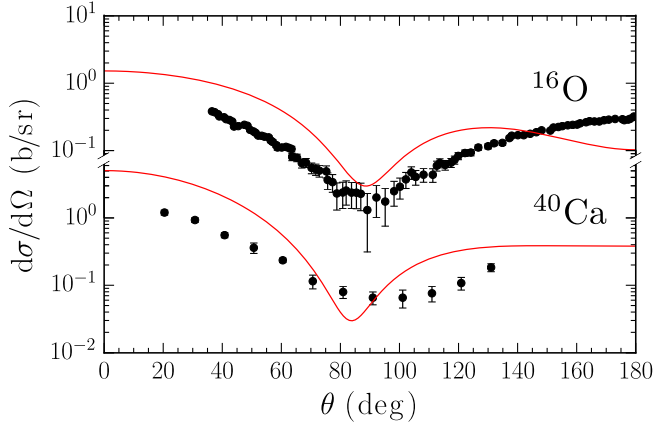
FIG. 3. Differential cross section for neutron elastic scattering off ^{16}O (^{40}Ca) at 3.286 (3.2) MeV of neutron energy, with NNLO$_{sat}$ and compared to the empirical data from Refs. [44,50].

FIG. 4. Total elastic cross section for neutron elastic scattering on ^{16}O form SCGF ADC(3) at different incident neutron energies compared to the experiment in Ref. [51]. The dashed, dotted-dashed, and solid lines correspond to the sole static self-energy $\Sigma^{(\infty)}$, to retaining 50% of the $2p1h$ and $2h1p$ doorway configurations and to the complete Eq. (2), respectively.

Virtual excitations of the target have the double effect of increasing the attraction of the real part of the optical potential (and hence lowering the single particle spectrum) and of generating a large number of narrow resonances. This is clearly seen in Fig. 2, which displays the phase shifts for neutron elastic scattering predicted by the whole self-energy of Eq. (2). Most of the virtual excitations responsible for this, especially at low energy, are accessed by coupling to hundreds of $2p1h$ configurations for ^{17}O and appear as clear spikes or "smoothed" oscillations in the figure. The SCGF-ADC(3) approach has the advantage of including these states naturally, even at large energies, so it describes efficiently the relevant physics. Table I compares the energies of some representative bound and scattering states to the experiment. The $3/2^+$ single particle resonance is computed at 0.91 MeV in the c.m. frame, very close to the experimental value. The first $1/2^-$ and $3/2^-$ are both predicted as bound states, although experimentally they are found inverted with the $3/2^-$ in the continuum. We calculate a narrow width for the $5/2^-$ and $7/2^-$ resonances, corresponding to excited states, close to the ones observed at 3.02 and 3.54 MeV [44]. However, there are other very narrow f-wave resonances, measured between 1.55 and 2.82 MeV, that our SCGF calculations do not resolve. In general, we find that NNLO$_{sat}$ predicts the location of dominant quasiparticle and hole states with an accuracy of $\lesssim 1$ MeV for this nucleus.

Figure 3 compares the low-energy differential cross sections originating from Eq. (5) to neutron scattering data for ^{16}O at 3.286 MeV and ^{40}Ca at 3.2 MeV. The minima are reproduced well for ^{16}O (and close to the experiment for ^{40}Ca), confirming the correct prediction of density distributions for NNLO$_{sat}$ [32,34,46]. However, the results are somewhat overestimated and hint at a general lack of absorption that is usually faced by attempts at computing the optical potentials *ab initio*. This is likely related to missing doorway configurations ($3p2h$ and beyond) that should be propagated in the denominators of Eq. (2) but are neglected by state-of-the-art approaches. Note that there are more than 200 experimentally observed excitations already between the ground state and the neutron separation threshold in ^{41}Ca [47], while the SCGF ADC(3) predicts only about 40 of them. This issue is likely to worsen at higher energies, where configurations more complex than $2p1h$ become relevant. We investigated this problem by computing total $n + ^{16}O$ elastic cross sections, $\sigma(E_{c.m.})$, with only $\Sigma^{(\infty)}$, suppressing 50% of the $2p1h$ and $2h1p$ states (evenly across all energies), and by using the complete ADC(3) self-energy. Figure 4 shows that $\sigma(E_{c.m.})$ presents oscillations up to about 5 MeV. These are in part reproduced by theory and are sensible to

TABLE I. Excitation spectrum of ^{17}O with respect to the $n + ^{16}O$ threshold, as obtained from Eq. (5) and the NNLO$_{sat}$ interaction and compared to the experiment [45]. Broad resonances in the continuum (most notably, the $5/2^+$) are computed at midpoint. The asterisk subscripts indicate higher excited states, above the lowest one, for each partial wave.

ε (MeV)	$5/2^+$	$1/2^+$	$1/2^-$	$5/2^-$	$3/2^-$	$3/2^+$	$5/2^+_*$	$5/2^-_*$	$7/2^-_*$
Exp	−4.14	−3.27	−1.09	−0.30	0.41	0.94	3.23	3.02	3.54
NNLO$_{sat}$	−5.06	−3.58	−0.15	−1.23	−2.24	0.91	4.57	3.36	3.37

interferences among the projectile and the included $2p1h$ configurations. However, the link between the absorption and the density of the intermediate doorway configurations becomes clear at higher energies, and it is confirmed by our calculations [48].

To conclude, we benchmarked optical potentials generated through SCGF theory to analogous full scale NCSMC simulations and to data for neutron elastic scattering at low energy. For both theory approaches, the correct asymptotic behavior of the scattering wave was reproduced even if the target wave function and the optical potentials were expanded in a HO basis. The theory benchmark, with freezing of virtual excitation of the target, is very encouraging. The SCGF approach also has the capability of accounting for a large number of such intermediate excitations up to very large energies, and it achieves a promising description of complex resonance states from first principles. The use of a saturating chiral interaction allows us to make a meaningful comparison to the experiment, which was not possible in previous investigation of this approach. Overall, we found that the most important features of optical potentials at low energy are well reproduced, together with key observables related to elastic scattering.

This Letter also puts into evidence how the lack of absorption normally observed in *ab initio* generated optical potentials is directly linked to the neglect of doorway configurations beyond $2p1h$ ones. Thus, addressing this challenge will be the next fundamental step toward predictive theories at medium scattering energies. It remains clear from the present results that obtaining reliable *ab initio* optical potentials, directly from the self-energy, is becoming a goal within reach. These findings open a path to establishing consistent theories of structure and reactions for medium mass nuclei.

[1] H. Feshbach, Ann. Phys. (N.Y.) **5**, 357 (1958).
[2] F. Capuzzi and C. Mahaux, Ann. Phys. (N.Y.) **245**, 147 (1996).
[3] L. S. Cederbaum, Ann. Phys. (N.Y.) **291**, 169 (2001).
[4] C. Mahaux, P. F. Bortignon, R. A. Broglia, and C. H. Dasso, Phys. Rep. **120**, 1 (1985).
[5] A. Idini, F. Barranco, and E. Vigezzi, Phys. Rev. C **85**, 014331 (2012).
[6] A. Idini, G. Potel, F. Barranco, E. Vigezzi, and R. A. Broglia, Phys. Rev. C **92**, 031304(R) (2015).
[7] R. A. Broglia, P. F. Bortignon, F. Barranco, E. Vigezzi, A. Idini, and G. Potel, Phys. Scr. **91**, 063012 (2016).
[8] C. H. Johnson and C. Mahaux, Phys. Rev. C **38**, 2589 (1988).
[9] R. J. Charity, L. G. Sobotka, and W. H. Dickhoff, Phys. Rev. Lett. **97**, 162503 (2006).
[10] W. H. Dickhoff, R. J. Charity, and M. H. Mahzoon, J. Phys. G **44**, 033001 (2017).
[11] G. Blanchon, M. Dupuis, H. F. Arellano, and N. Vinh Mau, Phys. Rev. C **91**, 014612 (2015).
[12] M. Vorabbi, P. Finelli, and C. Giusti, Phys. Rev. C **93**, 034619 (2016).
[13] M. Gennari, M. Vorabbi, A. Calci, and P. Navrátil, Phys. Rev. C **97**, 034619 (2018).
[14] M. Burrows, C. Elster, S. P. Weppner, K. D. Launey, P. Maris, A. Nogga, and G. Popa, Phys. Rev. C **99**, 044603 (2019).
[15] T. R. Whitehead, Y. Lim, and J. W. Holt, Phys. Rev. C **100**, 014601 (2019).
[16] K. Varga, S. C. Pieper, Y. Suzuki, and R. B. Wiringa, Phys. Rev. C **66**, 034611 (2002).
[17] K. M. Nollett, S. C. Pieper, R. B. Wiringa, J. Carlson, and G. M. Hale, Phys. Rev. Lett. **99**, 022502 (2007).
[18] J. E. Lynn, I. Tews, J. Carlson, S. Gandolfi, A. Gezerlis, K. E. Schmidt, and A. Schwenk, Phys. Rev. Lett. **116**, 062501 (2016).
[19] P. Navrátil, R. Roth, and S. Quaglioni, Phys. Rev. C **82**, 034609 (2010).
[20] S. Baroni, P. Navrátil, and S. Quaglioni, Phys. Rev. Lett. **110**, 022505 (2013).
[21] F. Raimondi, G. Hupin, P. Navrátil, and S. Quaglioni, Phys. Rev. C **93**, 054606 (2016).
[22] G. Hagen and N. Michel, Phys. Rev. C **86**, 021602(R) (2012).
[23] J. Rotureau, P. Danielewicz, G. Hagen, F. M. Nunes, and T. Papenbrock, Phys. Rev. C **95**, 024315 (2017).
[24] J. Rotureau, P. Danielewicz, G. Hagen, G. R. Jansen, and F. M. Nunes, Phys. Rev. C **98**, 044625 (2018).
[25] W. Dickhoff and C. Barbieri, Prog. Part. Nucl. Phys. **52**, 377 (2004).
[26] V. Somà, T. Duguet, and C. Barbieri, Phys. Rev. C **84**, 064317 (2011).
[27] C. Barbieri and B. K. Jennings, Phys. Rev. C **72**, 014613 (2005).
[28] S. Waldecker, C. Barbieri, and W. H. Dickhoff, Phys. Rev. C **84**, 034616 (2011).
[29] A. Carbone, A. Cipollone, C. Barbieri, A. Rios, and A. Polls, Phys. Rev. C **88**, 054326 (2013).
[30] A. Cipollone, C. Barbieri, and P. Navrátil, Phys. Rev. C **92**, 014306 (2015).
[31] F. Raimondi and C. Barbieri, Phys. Rev. C **97**, 054308 (2018).
[32] A. Ekström, G. R. Jansen, K. A. Wendt, G. Hagen, T. Papenbrock, B. D. Carlsson, C. Forssén, M. Hjorth-Jensen,

P. Navrátil, and W. Nazarewicz, Phys. Rev. C **91,** 051301(R) (2015).

[33] V. Lapoux, V. Somà, C. Barbieri, H. Hergert, J. D. Holt, and S. R. Stroberg, Phys. Rev. Lett. **117,** 052501 (2016).

[34] R. F. Garcia Ruiz *et al.* Nat. Phys. **12,** 594 (2016).

[35] N. Rocco and C. Barbieri, Phys. Rev. C **98,** 025501 (2018).

[36] J. Schirmer, L. S. Cederbaum, and O. Walter, Phys. Rev. A **28,** 1237 (1983).

[37] C. Barbieri and A. Carbone, in *An Advanced Course in Computational Nuclear Physics: Bridging the Scales from Quarks to Neutron Stars*, edited by M. Hjorth-Jensen, M. P. Lombardo, and U. van Kolck, Lecture Notes in Physics Vol. 936 (Springer, Cham, 2017), https://link.springer.com/chapter/10.1007%2F978-3-319-53336-0_11.

[38] J. Escher and B. K. Jennings, Phys. Rev. C **66,** 034313 (2002).

[39] G. Hagen, T. Papenbrock, and D. J. Dean, Phys. Rev. Lett. **103,** 062503 (2009).

[40] A. E. L. Dieperink and T. de Forest, Jr, Phys. Rev. C **10,** 543 (1974).

[41] D. R. Entem and R. Machleidt, Phys. Rev. C **68,** 041001 (2003).

[42] S. K. Bogner, R. J. Furnstahl, and R. J. Perry, Phys. Rev. C **75,** 061001(R) (2007).

[43] R. Roth and P. Navrátil, Phys. Rev. Lett. **99,** 092501 (2007).

[44] D. Lister and A. Sayres, Phys. Rev. **143,** 745 (1966).

[45] D. Tilley, H. Weller, and C. Cheves, Nucl. Phys. **A564,** 1 (1993).

[46] T. Duguet, V. Somà, S. Lecluse, C. Barbieri, and P. Navrátil, Phys. Rev. C **95,** 034319 (2017).

[47] C. Nesaraja and E. McCutchan, Nucl. Data Sheets **133,** 1 (2016).

[48] Note that the Lanczos algorithm used to solve for Eq. (2) does not affect these conclusions since it is specifically designed to preserve the strength distribution of response functions, see Refs. [28,49].

[49] V. Somà, C. Barbieri, and T. Duguet, Phys. Rev. C **89,** 024323 (2014).

[50] R. Becker, W. Guindon, and G. Smith, Nucl. Phys. **89,** 154 (1966).

[51] D. A. Brown *et al.*, Nucl. Data Sheets **148,** 1 (2018).